


Tidal deformability of crystallized white dwarfs in full general relativityL. Perot¹ and N. Chamel¹*Institute of Astronomy and Astrophysics, Université Libre de Bruxelles,
CP 226, Boulevard du Triomphe, B-1050 Brussels, Belgium* (Received 13 May 2022; accepted 16 June 2022; published 12 July 2022)

Space-based gravitational-wave detectors offer new prospects for probing the interior of white dwarfs in binary systems through the imprints of tidal effects on the gravitational-wave signal. Some of the binaries that will be observed could have evolved for long enough for the white dwarfs to be at least partially crystallized. The apsidal motion constant k_2 (also called the second gravitoelectric Love number) of a cold crystallized white dwarf is computed in full general relativity considering different compositions. The elasticity of the crystallized core is found to systematically reduce the tidal deformability, especially for low-mass stars. Fully relativistic results are compared to those obtained in Newtonian gravity. It is shown that the relativistic correction to the observable tidal deformability $k_2 R^5$ (where R is the stellar radius) is negligible for low-mass white dwarfs but becomes increasingly important for more massive white dwarfs. When approaching the maximum mass, the application of Newtonian theory instead of general relativity leads to dramatic errors. The case of eccentric binaries, for which the precession of the periastron causes a frequency splitting of the gravitational-wave signal depending on the apsidal motion constants of the two stars, is investigated. Future measurements of the precession rate by the Laser Interferometer Space Antenna, which is planned to be in operation within the next decade, could potentially provide estimates of the individual masses. It is found that the errors incurred by the neglect of the elasticity of the crystallized core could be very large, especially for low-mass white dwarfs. Gravitational-wave observations could thus provide a new way to study the crystallization of white dwarfs.

DOI: [10.1103/PhysRevD.106.023012](https://doi.org/10.1103/PhysRevD.106.023012)**I. INTRODUCTION**

The direct detection of gravitational waves (GWs) from the mergers of black holes and/or neutron stars by the LIGO-Virgo Collaboration has opened a new era in astronomy, offering a completely new way of probing the physics of these compact objects [1]. The advent of space-based GW observatories—such as the Laser Interferometer Space Antenna (LISA) [2], the Deci-hertz Interferometer Gravitational Wave Observatory [3], TianQin, and Taiji [4]—will allow the detection of signals with lower frequencies ranging from 10^{-4} to 10 Hz emitted by a variety of different sources, most of which are expected to be double white dwarfs (WDs) in our Galaxy. According to population synthesis models, more than 10^4 binaries could be individually resolved over the nominal 4-year duration of the LISA mission [5–8] (see also Ref. [9]). Among them, eccentric binaries are of particular interest for probing the structure of WDs and the properties of dense matter. Eccentric binaries may be formed through dynamical interactions in globular clusters [10] or as products of hierarchical triple systems [11]. For such binaries, tidal forces cause a non-dissipative precession of the periastron of the orbit. This so-called apsidal motion could be observable with LISA [12–14]. While in purely elliptic binaries GW radiation is emitted at multiples

of the orbital frequency (see, e.g., Sec. IV. 1.2 in Ref. [15]), in the presence of periastron precession each of these harmonics is split into a triplet with frequencies separated by $\dot{\gamma}/\pi$, where $\dot{\gamma}$ is the apsidal precession rate [12] (a dot is used to indicate a time derivative). The tidal contribution to $\dot{\gamma}$ is governed by the quadrupolar apsidal motion constant k_2 (also referred to as the Love number), which in turn is determined by the internal constitution of WDs. However, most binaries are expected to be circular and emit monochromatic GWs at twice the orbital frequency. Information on tidal effects and k_2 could still be potentially extracted from long-term monitoring of such systems [16–19].

Depending on their initial orbital period and eccentricities, the binaries that will be observed by LISA may have evolved for billions of years since their formation, a long enough time for the interior of the WDs to have crystallized at least partially. Predicted and studied independently by Kirzhnits [20], Abrikosov [21], and Salpeter [22], the crystallization of dense matter in the core of WDs first found observational evidence in 1997 from the asteroseismological study of BPM 37093 [23] (see, e.g., Ref. [24] for more recent developments). Crystallization was also shown to affect the cooling of a WD [25,26], but it was only recently that strong observational support was reported from the analysis of the GAIA data [27].

The crystallization of WDs is likely to alter their tidal deformability, which in turn could impact the orbital motion of binaries and the GW emission. However, previous studies, including recent calculations of the tidal deformability [28,29], assumed purely fluid WDs treated in Newtonian theory.

In this paper, we compute the quadrupolar apsidal motion constant k_2 of WDs in full general relativity (GR), allowing for the existence of a solid core by adapting the formalism developed in the neutron-star context [30–33]. The adopted equation of state is briefly described in Sec. II. After presenting the general-relativistic formalism in Sec. III, numerical results are discussed in Sec. IV.

All values for the fundamental constants were taken from NIST CODATA 2018.¹ We use the spacetime metric signature $(-, +, +, +)$.

II. EQUATION OF STATE FOR A WHITE DWARF

The core of a WD consists of a dense Coulomb plasma of atomic nuclei coexisting with a relativistic gas of free electrons. Apart from carbon and oxygen (the primary ashes of helium burning), the core may contain other nuclei like helium [34–36], neon, and magnesium [37]. The core of some WDs might even be made of iron. Iron WDs could be formed from the explosive ignition of electron-degenerate oxygen-neon-magnesium cores [38], or from failed-detonation supernovae [39]. However, observational evidence for the existence of such iron WDs remains elusive [40–47]. For simplicity, we will assume that the stellar core is made of only one type of nuclei with charge number Z and mass number A . The core of a WD is generally surrounded by a helium mantle and a hydrogen envelope. However, their contribution to the mass of the star cannot exceed $\sim 1\%$ and $\sim 0.01\%$, respectively, to avoid a thermonuclear runaway. We will ignore these layers here.

Crystallization of the core occurs at a temperature T_m , approximately given by [48]

$$T_m \approx 1.3 \times 10^5 Z^2 \left(\frac{175}{\Gamma_m} \right) \left(\frac{\rho_6}{A} \right)^{1/3} \text{ K}, \quad (1)$$

where k_B is Boltzmann's constant, $\Gamma_m \approx 175$ is the Coulomb coupling parameter at melting (see, e.g., Ref. [49] and references therein for a discussion of corrections), and $\rho_6 = \rho/10^6 \text{ g cm}^{-3}$, where ρ is the mass-energy density. We will consider that the WD has sufficiently cooled down such that the core has crystallized. The core of He WDs might form a Bose-Einstein condensate instead [50]; however, a crystalline phase is not excluded either [51]. Because the temperature T_m is much lower than the electron Fermi temperature, defined by

$$T_{Fe} = \frac{\mu_e - m_e c^2}{k_B} \approx 6.0 \times 10^9 \left(\frac{Z}{A} \rho_6 \right)^{1/3} \text{ K}, \quad (2)$$

where μ_e is the electron Fermi energy, m_e is the electron mass, and c is the speed of light, electrons are highly degenerate in the core of a crystallized WD. To a good approximation, electrons can therefore be treated as a relativistic Fermi gas. We will neglect the thermal contributions to the thermodynamic potentials.

Since the Coulomb crystal is electrically neutral, the number density n_i of ions is directly determined by the electron density n_e through $n_i = n_e/Z$. The mass density is thus given by

$$\rho_N = n_e \frac{M(A, Z)}{Z}, \quad (3)$$

where the nucleus mass $M(A, Z)$ (including the rest mass of Z electrons) can be obtained from the corresponding tabulated atomic mass excess $E(A, Z)$ after subtracting out the electron binding energy as follows [52]:

$$M(A, Z) = Am_u + E(A, Z) + 1.44381 \times 10^{-5} Z^{2.39} + 1.55468 \times 10^{-12} Z^{5.35}, \quad (4)$$

where m_u is the unified atomic mass unit. The baryon number density is given by

$$n = \frac{A}{Z} n_e = An_i. \quad (5)$$

Taking into account lattice, electron exchange, and screening corrections, the mass-energy density ρ and pressure P of the one-component Coulomb crystal are approximately given, respectively, by [53]

$$\rho = \rho_N + \frac{m_e}{8\pi^2 \lambda_e^3} \left[x_r (1 + 2x_r^2) \sqrt{1 + x_r^2} - \log \left(x_r + \sqrt{1 + x_r^2} \right) \right] \times \left(1 + \frac{\alpha}{2\pi} \right) - n_e m_e + C_M \left(\frac{4\pi}{3} \right)^{1/3} \frac{\alpha \hbar}{c} n_e^{4/3} Z_{\text{eff}}^{2/3}, \quad (6)$$

$$P = \frac{m_e c^2}{8\pi^2 \lambda_e^3} \left[x_r \left(\frac{2}{3} x_r^2 - 1 \right) \sqrt{1 + x_r^2} + \log \left(x_r + \sqrt{1 + x_r^2} \right) \right] \times \left(1 + \frac{\alpha}{2\pi} \right) + \frac{C_M}{3} \left(\frac{4\pi}{3} \right)^{1/3} \alpha \hbar c n_e^{4/3} Z_{\text{eff}}^{2/3}, \quad (7)$$

where $x_r = \lambda_e k_e$ is a dimensionless relativity parameter with the electron Compton wavelength $\lambda_e = \hbar/(m_e c)$ and electron Fermi wave number $k_e = (3\pi^2 n_e)^{1/3}$, \hbar is the reduced Planck constant, α is the fine-structure constant, C_M is the Madelung constant, and

$$Z_{\text{eff}} \equiv Z \sigma(Z)^{3/2} \quad (8)$$

¹<https://physics.nist.gov/cuu/Constants/>.

with the dimensionless function

$$\sigma(Z) \equiv 1 + \alpha \frac{12^{4/3}}{35\pi^{1/3}} (1 - 1.1866Z^{-0.267} + 0.27Z^{-1})Z^{2/3}. \quad (9)$$

The introduction of an effective nuclear charge Z_{eff} is to approximately account for electron charge screening effects, as discussed in Ref. [53]. Considering that ions are arranged in a body-centered cubic lattice, as predicted by *ab initio* density functional calculations for carbon [54], the Madelung constant is given by $C_M = -0.895929255682$ [55].

At the scales of interest for the global description of tidal deformations, we assume that each stellar matter element consists of an isotropic polycrystalline solid. The elastic properties are thus characterized by a single parameter, the effective shear modulus, given by [56,57]

$$\tilde{\mu} = 0.119457234091 \left(\frac{4\pi}{3}\right)^{1/3} \alpha \hbar c Z^{2/3} n_e^{4/3}. \quad (10)$$

This value, obtained from a Voigt average, represents an upper limit [58].

III. RELATIVISTIC TIDAL DEFORMATIONS OF AN ELASTIC STAR

A WD in a close orbit with a compact companion is tidally deformed by the mutual gravitational interactions. Assuming internal motions are much faster than orbital motions (adiabatic approximation), the static external quadrupolar tidal field \mathcal{E}_{ij} induces a nonzero quadrupolar mass moment Q_{ij} in the star, which is given to linear order by [59]

$$Q_{ij} = \frac{2}{3G} k_2 R^5 \mathcal{E}_{ij}, \quad (11)$$

where G is the universal gravitational constant, R is the stellar radius, and the second gravitoelectric Love number k_2 is a dimensionless parameter characterizing the tidal response of the star.

A. Background configuration

During most of the binary evolution, tidal effects remain negligible (see, e.g., Ref. [60] for a review). They come into play only during the last stage (observable by space-based gravitational-wave detectors) after a time presumably long enough for the WDs to have crystallized, as will be further discussed in Sec. IV D. Considering that the WDs are nonrotating, we can thus reasonably assume that their solid interior is not strained when tidal interactions start to become significant. The stress-energy tensor of a fully relaxed solid star takes the same form as for a perfect fluid star,

$$T_\mu^\nu = (P + \rho c^2) u_\mu u^\nu + P \delta_\mu^\nu, \quad (12)$$

where u^μ denotes the fluid four-velocity. The spacetime metric can be written as

$$g_{\mu\nu} = \text{diag}\{-e^\nu, e^\lambda, r^2, r^2 \sin^2 \theta\}, \quad (13)$$

where $\nu = \nu(r)$ and $\lambda = \lambda(r)$ depend only on the radial coordinate r . Given the normalization relation $u_\mu u^\mu = -1$, the four-velocity of the fluid inside the static star and the stress-energy tensor are explicitly given by

$$u^\mu = (e^{-\nu/2}, 0, 0, 0) \quad (14)$$

and

$$T_\mu^\nu = \text{diag}\{-\rho c^2, P, P, P\}, \quad (15)$$

respectively. Setting

$$e^\lambda = \left(1 - \frac{2Gm}{c^2 r}\right)^{-1}, \quad (16)$$

solving the Einstein field equations leads to the Tolman-Oppenheimer-Volkoff (TOV) equations [61,62],

$$m' = 4\pi r^2 \rho, \quad (17a)$$

$$P' = -\frac{1}{2}(P + \rho c^2)\nu', \quad (17b)$$

where the prime denotes a derivative with respect to r and $m(r)$ represents the gravitational mass enclosed in a sphere of radius r . The metric potentials are given by

$$\nu' = e^\lambda \left(\frac{2Gm}{c^2 r^2} + 8\pi r \frac{G}{c^4} P \right), \quad (17c)$$

$$\lambda' = e^\lambda \left(-\frac{2Gm}{c^2 r^2} + 8\pi r \frac{G}{c^2} \rho \right). \quad (17d)$$

The radial coordinate R delimiting the stellar surface and defining the circumferential radius of the star is determined by the condition $P(R) = 0$. The gravitational mass of the star is then defined as $M = m(R)$.

In the Newtonian limit, the TOV equations reduce to the classical hydrostatic equilibrium equations:

$$m' = 4\pi r^2 \rho_N, \quad (18a)$$

$$P' = -\frac{Gm\rho_N}{r^2}, \quad (18b)$$

with the mass density ρ_N given by Eq. (3).

B. Tidal perturbations

We will now review the formalism to determine static gravitoelectric (even-parity) tidal perturbations following the analogous study of Ref. [32] in the neutron-star context.

Since we consider an unstrained background, the stellar elasticity manifests itself only in the perturbed configuration. To solve the elastic problem, we have to consider the perturbations of the total stress-energy tensor obtained by adding the contribution $\delta\Pi_\mu^\nu$ of the shear tensor to variations of the perfect-fluid stress-energy tensor (12). The perturbed Einstein field equations thus become

$$\delta G_\mu^\nu = \frac{8\pi G}{c^4} \delta T_{\mu\text{tot}}^\nu = \frac{8\pi G}{c^4} (\delta T_\mu^\nu + \delta\Pi_\mu^\nu). \quad (19)$$

From Eq. (12), the perturbed perfect-fluid stress-energy tensor is given by

$$\begin{aligned} \delta T_\mu^\nu &= (\delta P + \delta\rho c^2) u_\mu u^\nu + (P + \rho c^2) (\delta u_\mu u^\nu + u_\mu \delta u^\nu) \\ &\quad + \delta P \delta_\mu^\nu. \end{aligned} \quad (20)$$

Since the equation of state is barotropic, i.e., the mass-energy density (6) and pressure (7) are functions of the baryon number density only, their Euler variations are simply given by

$$\delta P = \frac{dP}{d\rho} \delta\rho, \quad \delta\rho = \frac{d\rho}{dn} \delta n, \quad (21)$$

where $c^2 \frac{d\rho}{dn} = \mu$ is the baryon chemical potential, and $\frac{dP}{d\rho} = c_s^2$ is the squared speed of sound. The latter relation implies in particular that

$$\delta P = c_s^2 \delta\rho. \quad (22)$$

The perturbed perfect-fluid stress-energy tensor is thus explicitly given by

$$\delta T_\mu^\nu = \text{diag} \left\{ -\frac{c^2}{c_s^2}, 1, 1, 1 \right\} \delta P. \quad (23)$$

In the Regge-Wheeler gauge [63], the static Eulerian perturbation of the metric is given by

$$\delta g_{\mu\nu} \equiv h_{\mu\nu} = \text{diag} \{ e^\nu H_0, e^\lambda H_2, r^2 K, r^2 \sin^2 \theta K \} Y_{\ell m}, \quad (24)$$

where $H_0 = H_0(r)$, $H_2 = H_2(r)$, and $K = K(r)$ are radial functions describing the perturbed spacetime and $Y_{\ell m} = Y_{\ell m}(\theta, \phi)$ is a spherical harmonic. Note that, in the following, all of the perturbed quantities will be factored into a radial and an angular part in a similar way. The small changes in the coordinates are described by

$$r \rightarrow r + \xi^r, \quad \theta \rightarrow \theta + \xi^\theta, \quad \phi \rightarrow \phi + \xi^\phi, \quad (25)$$

where the components of the static displacement vector ξ^μ are written as

$$\xi^\mu = \left(0, \frac{W}{r}, \frac{V}{r^2} \frac{\partial}{\partial \theta}, \frac{V}{r^2 \sin^2 \theta} \frac{\partial}{\partial \phi} \right) Y_{\ell m}, \quad (26)$$

with the functions $W = W(r)$ and $V = V(r)$ describing the radial and tangential displacements, respectively.

The Lagrangian variation of the fluid four-velocity is given by [64]

$$\Delta u^\mu = \frac{1}{2} u^\mu u^\nu u^\sigma \Delta g_{\nu\sigma}. \quad (27)$$

Since the Lagrangian variations are related to the Eulerian ones through $\Delta = \delta + \mathcal{L}_\xi$, where \mathcal{L}_ξ represents the Lie derivative along ξ^μ , the Lagrangian variation of the metric reads $\Delta g_{\mu\nu} = h_{\mu\nu} + \mathcal{L}_\xi g_{\mu\nu}$, and the Eulerian variation of the fluid four-velocity is thus given by

$$\delta u^\mu = \frac{1}{2} u^\mu u^\nu u^\sigma h_{\nu\sigma} + \perp_\nu^\mu \mathcal{L}_u \xi^\nu, \quad (28)$$

where the orthogonal projector to the fluid flow is $\perp_{\mu\nu} = g_{\mu\nu} + u_\mu u_\nu$, and \mathcal{L}_u represents the Lie derivative along the fluid four-velocity. Its explicit components are

$$\delta u^\mu = \left(\frac{e^{-\nu/2}}{2} H_0, 0, 0, 0 \right) Y_{\ell m}. \quad (29)$$

The Lagrangian variations of the pressure and mass-energy density are simply given by

$$\Delta P = \frac{dP}{d\rho} \Delta\rho, \quad \Delta\rho = \frac{d\rho}{dn} \Delta n, \quad (30)$$

and the Lagrangian variation of the density n is [64]

$$\Delta n = -\frac{1}{2} n \perp^{\mu\nu} \Delta g_{\mu\nu}, \quad (31)$$

which explicitly reads

$$\begin{aligned} \Delta n &= \frac{n}{r^2} \left[\ell(\ell+1)V - rW' \right. \\ &\quad \left. - \left(1 + \frac{r\lambda'}{2} \right) W - r^2 \left(K + \frac{H_2}{2} \right) \right] Y_{\ell m}. \end{aligned} \quad (32)$$

Finally, using the Gibbs-Duhem relation $\rho c^2 + P = \mu n$ together with Eq. (32) inserted into Eqs. (30) yields

$$\begin{aligned} \Delta P &= \frac{(P + \rho c^2) c_s^2}{r^2 c^2} \left[\ell(\ell+1)V - rW' \right. \\ &\quad \left. - \left(1 + \frac{r\lambda'}{2} \right) W - r^2 \left(K + \frac{H_2}{2} \right) \right] Y_{\ell m}. \end{aligned} \quad (33)$$

From the relation between the Lagrangian and Eulerian variations and using the TOV equation (17b) for the pressure, we also have

$$\Delta P = \left(\delta P - \frac{P + \rho c^2}{2r} \nu' W \right) Y_{\ell m}, \quad (34)$$

where here and in the following $\delta P = \delta P(r)$ denotes the radial part of the perturbed pressure [with the full perturbation being given by $\delta P(r) Y_{\ell m}(\theta, \phi)$]. The combination of the two latter relations will be useful to close the system of differential equations for the elastic problem.

The perturbed shear tensor is given by [65]

$$\delta \Pi_{\mu}^{\nu} = -\tilde{\mu} \left(\perp_{\mu}^{\sigma} \perp^{\nu \rho} - \frac{1}{3} \perp_{\mu}^{\nu} \perp^{\sigma \rho} \right) \Delta g_{\sigma \rho}. \quad (35)$$

As in Refs. [30,32], we define the dimensionless radial and tangential traction variables $T_r = T_r(r)$ and $T_{\theta} = T_{\theta}(r)$ as follows:

$$\begin{aligned} T_r Y_{\ell m} &= \frac{G}{c^4} r^2 \delta \Pi_r^r \\ &= -\frac{2G}{3c^4} \tilde{\mu} [2rW' + (r\lambda' - 4)W + \ell(\ell + 1)V \\ &\quad + r^2(H_2 - K)] Y_{\ell m}, \end{aligned} \quad (36)$$

$$\begin{aligned} T_{\theta} \frac{\partial Y_{\ell m}}{\partial \theta} &= \frac{G}{c^4} r^3 \delta \Pi_r^{\theta} \\ &= -\frac{G}{c^4} \tilde{\mu} (rV' - 2V + e^{\lambda} W) \frac{\partial Y_{\ell m}}{\partial \theta}. \end{aligned} \quad (37)$$

With these definitions, the nonzero components of the perturbed shear tensor are

$$\delta \Pi_r^r = \frac{c^4 T_r}{G r^2} Y_{\ell m}, \quad (38a)$$

$$\delta \Pi_r^{\theta} = \frac{e^{\lambda}}{r^2} \delta \Pi_{\theta}^r = \frac{c^4 T_{\theta}}{G r^3} \frac{\partial Y_{\ell m}}{\partial \theta}, \quad (38b)$$

$$\delta \Pi_r^{\phi} = \frac{e^{\lambda}}{r^2 \sin^2 \theta} \delta \Pi_{\phi}^r = \frac{c^4 T_{\theta}}{G r^3 \sin^2 \theta} \frac{\partial Y_{\ell m}}{\partial \phi}, \quad (38c)$$

$$\delta \Pi_{\theta}^{\theta} = -\left\{ \frac{\tilde{\mu} V}{r^2} \left[\ell(\ell + 1) + 2 \frac{\partial^2}{\partial \theta^2} \right] + \frac{1}{2} \frac{c^4 T_r}{G r^2} \right\} Y_{\ell m}, \quad (38d)$$

$$\delta \Pi_{\phi}^{\phi} = \left\{ \frac{\tilde{\mu} V}{r^2} \left[\ell(\ell + 1) + 2 \frac{\partial^2}{\partial \theta^2} \right] - \frac{1}{2} \frac{c^4 T_r}{G r^2} \right\} Y_{\ell m}, \quad (38e)$$

$$\delta \Pi_{\phi}^{\theta} = \sin^2 \theta \delta \Pi_{\theta}^{\phi} = \frac{2\tilde{\mu} V}{r^2} \left(\cot \theta \frac{\partial}{\partial \phi} - \frac{\partial^2}{\partial \theta \partial \phi} \right) Y_{\ell m}. \quad (38f)$$

Combining these with the perturbed Einstein field equations (19) leads to the following relation:

$$H_2 = H_0 + 32\pi \frac{G}{c^4} \tilde{\mu} V. \quad (39)$$

The definitions of the traction variables (36) and (37) together with Eq. (39) lead to two differential equations for V and W :

$$V' = \frac{2}{r} V - \frac{e^{\lambda}}{r} W - \frac{c^4 T_{\theta}}{G r \tilde{\mu}}, \quad (40a)$$

$$\begin{aligned} W' &= \left(\frac{2}{r} - \frac{\lambda'}{2} \right) W + \frac{r}{2} (K - H_0) - \frac{3c^4 T_r}{4G r \tilde{\mu}} \\ &\quad - \left[16\pi \frac{G}{c^4} r \tilde{\mu} + \frac{\ell(\ell + 1)}{2r} \right] V. \end{aligned} \quad (40b)$$

Defining

$$H'_0 = \beta, \quad (40c)$$

other appropriate combinations of the Einstein field equations lead to the following differential equations for K , T_{θ} , and β :

$$K' = \beta + \nu' H_0 + \frac{16\pi G}{r c^4} (2 + r\nu') \tilde{\mu} V - \frac{16\pi}{r} T_{\theta}, \quad (40d)$$

$$\begin{aligned} T'_{\theta} &= \left(\frac{\lambda' - \nu'}{2} - \frac{1}{r} \right) T_{\theta} - r e^{\lambda} \frac{G}{c^4} \delta P + \frac{1}{16\pi} (\nu' + \lambda') H_0 \\ &\quad + \frac{G e^{\lambda}}{c^4 r} [2 - \ell(\ell + 1)] \tilde{\mu} V + \frac{e^{\lambda}}{2r} T_r, \end{aligned} \quad (40e)$$

$$\begin{aligned} \beta' &= \left(\frac{\lambda' - \nu'}{2} - \frac{2}{r} \right) \beta \\ &\quad - \left\{ \frac{2}{r^2} - [2 + \ell(\ell + 1)] \frac{e^{\lambda}}{r^2} + \frac{3\nu' + \lambda'}{r} - \nu'^2 \right\} H_0 \\ &\quad - 8\pi \frac{G}{c^4} \left[e^{\lambda} \left(3 + \frac{c^2}{c_s^2} \right) \delta P + 2\nu' \tilde{\mu}' V \right. \\ &\quad \left. + 8 \left(\frac{1 - e^{\lambda}}{r^2} + \frac{3\nu' + \lambda'}{2r} - \frac{\nu'^2}{4} \right) \tilde{\mu} V - 2 \frac{e^{\lambda}}{r} \nu' \tilde{\mu} W \right]. \end{aligned} \quad (40f)$$

They also lead to the following algebraic relation involving δP and T_r :

$$\begin{aligned} \delta P &= \frac{1}{16\pi r^2 e^{\lambda} G} \left\{ r^2 \nu' \beta + [\ell(\ell + 1) e^{\lambda} - 2 + r^2 \nu'^2] H_0 \right. \\ &\quad \left. + [2 - \ell(\ell + 1)] e^{\lambda} K + 16\pi \frac{G}{c^4} r^2 \nu'^2 \tilde{\mu} V \right. \\ &\quad \left. - 16\pi (2 + r\nu') T_{\theta} - 16\pi e^{\lambda} T_r \right\}. \end{aligned} \quad (40g)$$

To close the system, we need one more relation involving δP and T_r . To this end, we combine Eqs. (33) and (34), using Eqs. (39) and (40b):

$$T_r = \frac{4G}{3c^4} \tilde{\mu} \left[\frac{r^2 c^2}{(P + \rho c^2) c_s^2} \delta P + \frac{3}{2} r^2 K - \frac{3}{2} \ell(\ell + 1) V + \left(3 - \frac{r v' c^2}{2c_s^2} \right) W \right]. \quad (40h)$$

The system of equations (40a)–(40h) fully determines the elastic perturbations. Note that all of our equations fully agree with Eqs. (30a)–(30g) of Ref. [32].

In the purely perfect fluid case, combining Eqs. (40e) and (40f) and setting $\tilde{\mu} = 0$ leads to the following perturbation equation for β :

$$\beta' = \left(\frac{\lambda' - \nu'}{2} - \frac{2}{r} \right) \beta - \left\{ \frac{2}{r^2} - [2 + \ell(\ell + 1)] \frac{e^\lambda}{r^2} + \frac{9\nu' + 5\lambda'}{2r} + \frac{(\nu' + \lambda')c^2}{2rc_s^2} - \nu'^2 \right\} H_0. \quad (41)$$

This equation coincides with Eq. (15) of Ref. [59] using the definition (40c). In the Newtonian limit, Eq. (41) reduces to

$$\beta' = -\frac{2}{r} \beta - \left[\frac{4\pi G \rho_N}{c_s^2} - \frac{\ell(\ell + 1)}{r^2} \right] H_0. \quad (42)$$

C. Tidal Love number and deformability

In our analysis, we will focus on the case $\ell = 2$. Introducing the dimensionless quantity

$$y = \frac{R\beta(R)}{H_0(R)} \quad (43)$$

evaluated at the surface of the star, the second gravito-electric Love number is given by [59]

$$k_2 = \frac{8}{5} C^5 (1 - 2C)^2 [2(y - 1)C - y + 2] \times \{ 2C[4(y + 1)C^4 + 2(3y - 2)C^3 - 2(11y - 13)C^2 + 3(5y - 8)C - 3(y - 2)] + 3(1 - 2C)^2 [2(y - 1)C - y + 2] \log(1 - 2C) \}^{-1}, \quad (44)$$

where $C = \frac{GM}{c^2 R}$ is the compactness parameter. The observable tidal deformability parameter is related to the Love number through

$$\Lambda_2 = \frac{2}{3} k_2 C^{-5}. \quad (45)$$

The Newtonian limit $C \rightarrow 0$ of Eq. (44) yields

$$k_2^N = \frac{2 - y}{2y + 6}. \quad (46)$$

As shown in Appendix B, k_2^N coincides with the so-called apsidal-motion constant discussed in previous studies. The Love number characterizes the distribution of matter inside the star: the more matter is concentrated, the lower k_2^N is. The highest possible value is thus reached for an incompressible star and is given by $k_2^N = 3/4$ [66].

D. Boundary conditions

Unlike neutron stars considered in Refs. [32,33] and made of an elastic crust on top of a liquid core, partially crystallized WDs are expected to have a solid core surrounded by some fluid layers. Following the approach of Refs. [32,33], we present here the boundary conditions that must be applied inside a WD: at the center, at the interface between the elastic and fluid regions, as well as at the surface.

1. Conditions at the stellar center

To solve the system of equations describing the structure of the star and the tidal perturbations presented in Secs. III A and III B, we need to specify the density ρ_c , pressure P_c , and shear modulus $\tilde{\mu}_c$ at the center of the star. Since the equations are singular in $r = 0$ due to the use of Schwarzschild coordinates (terms in $1/r$), we expand all fields $F(r)$ in series of the form

$$F(r) = r^s [F^{(0)} + F^{(2)} r^2 + \mathcal{O}(r^4)]. \quad (47)$$

Note that first-order terms in this expansion vanish due to the symmetry of the field equations. Explicit forms of the coefficients $F^{(0)}$ and $F^{(2)}$ and the exponents s are given in Appendix A. In the elastic case, we are left with three undetermined coefficients: one is an arbitrary amplitude, which cancels in the expression for the Love number (the tidal deformability does not depend on the amplitude of the perturbation), while the two others are to be determined using the boundary conditions at the surface of the elastic region.

2. Conditions at interfaces

At an elastic-fluid interface inside the star or at an elastic-vacuum interface (the stellar surface), the shear modulus $\tilde{\mu}$ varies discontinuously. There can also exist density discontinuities. In particular, the vanishing of the pressure at the surface of the star entails a finite density and a finite shear modulus, as can be seen from Eqs. (7) and (10). We shall thus consider generic boundary conditions allowing for discontinuities of both $\tilde{\mu}$ and ρ .

Following Ref. [32], imposing the continuity of the induced three-metric on the interface as well as the continuity of the extrinsic curvature, and making use of the appropriate Einstein field equations (40) lead to the following conditions:

$$\begin{aligned}
[T_\theta] = 0, \quad \left[T_r + \frac{G}{c^4} r^2 \delta P - \frac{1}{2c^2} \nu' r \rho W \right] = 0, \quad [W] = 0, \\
[K] = 0, \quad [H_0] = 0, \quad \left[\beta + 16\pi \frac{G}{c^4} \nu' \tilde{\mu} V - 8\pi \frac{G}{c^2} \frac{e^\lambda}{r} \rho W \right] = 0,
\end{aligned} \tag{48}$$

where we have introduced the notation $[F] = \lim_{\epsilon \rightarrow 0} [F(r + \epsilon) - F(r - \epsilon)]$. If the WD is only partially crystallized up to some radial coordinate $r = R_c$, the relevant associated boundary conditions read explicitly

$$\begin{aligned}
T_\theta^- = 0, \\
\frac{G}{c^4} R_c^2 (\delta P^+ - \delta P^-) - T_r^- - \frac{1}{2c^2} \nu'(R_c) R_c (\rho^+ - \rho^-) W(R_c) = 0,
\end{aligned} \tag{49}$$

$$\begin{aligned}
H_0^+ = H_0^-, \\
\beta^+ = \beta^- + 16\pi \frac{G}{c^4} \nu'(R_c) \tilde{\mu}^- V^- + 8\pi \frac{G}{c^2} \frac{e^{\lambda(R_c)}}{R_c} (\rho^+ - \rho^-) W(R_c),
\end{aligned} \tag{50}$$

where the “−” (“+”) refers to a quantity calculated at $r = R_c$ from the inner elastic (outer fluid) region. The same set of conditions can be applied at the surface of the star with $\rho^+ = 0$ and $\delta P^+ = 0$.

IV. NUMERICAL RESULTS

A. Numerical computations

1. Numerical scheme

We have solved the system of first-order differential equations (40) together with Eqs. (17) using the classical fourth-order Runge-Kutta method by integrating from the center of the star to the top of the elastic region. To avoid singularities, we have begun the integration at a small radial coordinate $r = \epsilon$ with initial conditions given by Eq. (47). Since the initial conditions depend on three unknown coefficients $H_0^{(0)}$, $V^{(0)}$, and $V^{(2)}$, we have generated three linearly independent solutions by setting $(H_0^{(0)}, V^{(0)}, V^{(2)}) = (1, 0, 0)$, $(0, 1, 0)$, and $(0, 0, 1)$, respectively. When superposing the solutions, one of the constants must be left arbitrary (arbitrary amplitude of the perturbation), and the two others are to be determined using the boundary conditions on the tractions (49). If a fluid layer is present on top of the elastic core, the two remaining boundary conditions (50) are to be used to pursue the integration to the stellar surface and to calculate the quantity $y(R)$ [Eq. (43)]; if not, these latter conditions are directly used to calculate $y(R)$. Note that the only density discontinuity that we consider here is at the stellar surface, recalling that the surface density is taken such that the pressure vanishes in Eq. (7).

2. Tests of our computer code

We have tested the precision of our computer code by considering purely fluid stars (with $\tilde{\mu} = 0$ everywhere) in Newtonian gravity using polytropic equations of state of the form (where \mathcal{K} and Γ are constants)

$$P = \mathcal{K} \rho_N^\Gamma, \tag{51}$$

for which solutions of the hydrostatic equilibrium equations (18a)–(18b) are known [67]. Love numbers k_ℓ^N (also called apsidal constants of motion; see Appendix B) were calculated for different values of the adiabatic index Γ in Ref. [66], recalling that physical solutions only exist for $\Gamma > 6/5$.

Given the density ρ_c at the center of the star, the mass and radius are expressible as [67]

$$M = 4\pi \left[\frac{\Gamma \mathcal{K}}{4\pi G(\Gamma - 1)} \right]^{3/2} \rho_c^{(3\Gamma-4)/2} \xi_1^2 |\theta'(q_1)|, \tag{52}$$

$$R = \sqrt{\frac{\Gamma \mathcal{K}}{4\pi G(\Gamma - 1)}} \rho_c^{(\Gamma-2)/2} q_1, \tag{53}$$

where $\theta(q)$ is the solution of the Lane-Emden equation

$$\frac{1}{q^2} \frac{d}{dq} q^2 \frac{d\theta}{dq} = -\theta^{1/(\Gamma-1)}, \tag{54}$$

with $\theta(0) = 1$ and $\theta'(0) = 0$ (the prime denoting here a derivative with respect to q), and q_1 is defined by $\theta(q_1) = 0$. Solutions for different values of Γ can be found in Ref. [67]. Love numbers k_ℓ^N are given by [66]

$$k_\ell^N = \frac{\ell + 1 - \eta(q_1)}{2\ell + 2\eta(q_1)}, \tag{55}$$

where $\eta(q)$ is the solution of the Clairaut-Radau equation

$$q\eta' + \eta(\eta - 1) - \ell(\ell + 1) + 2q \frac{\theta^{1/(\Gamma-1)}}{|\theta'|} (\eta + 1) = 0, \tag{56}$$

subject to the boundary condition $\eta(0) = \ell - 2$. It should be noted that the functions $\eta(q)$ and $\theta(q)$ depend on the equation of state only through the adiabatic index Γ but are independent of \mathcal{K} . Moreover, they do not depend on ρ_c . As a consequence, Love numbers k_ℓ^N are uniquely determined by ℓ and Γ and take the same values for all stars irrespective of their mass. For the special case $\Gamma = 2$, Eq. (56) for $\ell = 2$ can be recast into a Bessel equation and the Love number is given by [59]

$$k_2^N = \frac{15}{2\pi^2} - \frac{1}{2} = 0.259908877\dots \tag{57}$$

With our code, we have numerically solved Eqs. (18) and (42), setting $\Gamma = 2$ and using some arbitrary value for \mathcal{K} . Our numerical result for the Love number (46) agrees with the exact value (57) up to nine significant digits.

We have also compared our numerical results with those obtained when treating electrons in the ultrarelativistic regime $x_r \gg 1$, since in this case the equation of state (7) reduces to the polytropic form (51) with $\Gamma = 4/3$ and

$$\mathcal{K} = \mathcal{K}_0 \left[1 + \frac{\alpha}{2\pi} + \alpha \frac{4C_M}{3} \left(\frac{4}{9\pi} \right)^{1/3} Z_{\text{eff}}^{2/3} \right], \quad (58)$$

where

$$\mathcal{K}_0 = \frac{\hbar c (3\pi^2)^{1/3}}{4} \left(\frac{Z}{M(A, Z)} \right)^{4/3} \quad (59)$$

is the constant obtained in the original Chandrasekhar model [68] when considering an ideal electron Fermi gas ignoring electron exchange, as well as electrostatic and polarization corrections. The results obtained from our code agree with the mass and radius given by Eqs. (52) and (53) using the well-known solution $q_1 \simeq 6.89685$ and $q_1^2 |\theta'(q_1)| \simeq 2.01824$, up to six significant digits at least.

Finally, to assess the numerical stability of our elastic computer code, we have checked that the results for the Love number are independent of the chosen value for the lower radial coordinate ϵ in the integration, provided the value of ϵ does not exceed $\sim 1\%$ of the stellar radius R . Moreover, we have found that the results converge to the perfect-fluid values when the shear modulus goes to zero.

B. Effects of crystallization on the tidal deformability

To assess the impact of crystallization on the tidal deformability of a WD, we compare results obtained in full GR for stars that are either entirely solid or entirely fluid.

In Figs. 1–6, we show the second gravitoelectric tidal Love number k_2 as a function of the WD mass M with and without elasticity and the corresponding relative deviation, for WDs made of ${}^4\text{He}$, ${}^{12}\text{C}$, ${}^{16}\text{O}$, ${}^{20}\text{Ne}$, ${}^{24}\text{Mg}$, and ${}^{56}\text{Fe}$, respectively. First, we can see that, regardless of the composition and the mass, the inclusion of the elasticity of dense matter systematically reduces the Love number, similarly with the results obtained in neutron stars [30–33]. For a given mass, the relative difference in k_2 between the elastic and fluid models increases with the atomic number Z . This is not surprising as the shear modulus varies as $\sim Z^{2/3}$; see Eq. (10). The effect of crystallization is then the least (most) pronounced for helium (iron) WDs; as an example, for a $0.3 M_\odot$ star, the relative differences are about 2.1%, 5.5%, and 11% for helium, oxygen, and iron WDs, respectively. For a given composition, the less massive the star, the more significant the effects of elasticity. Note that the relative impact of crystallization

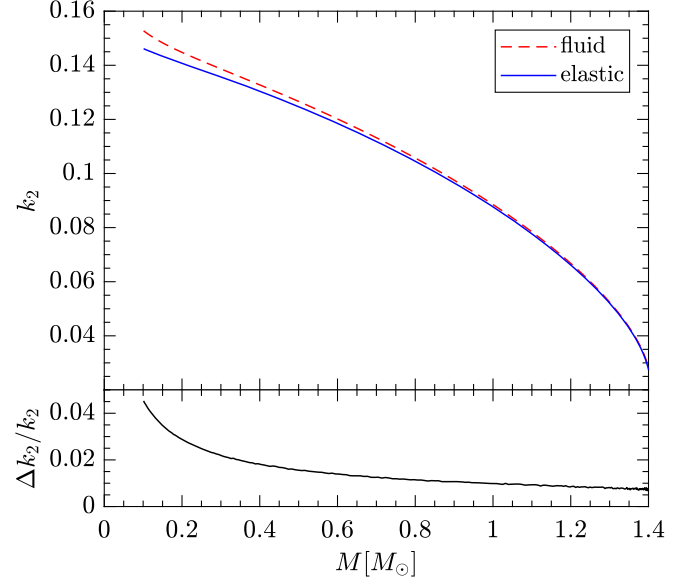


FIG. 1. Top panel: second gravitoelectric Love number k_2 as a function of the WD mass M with and without elasticity, for a WD made of ${}^4\text{He}$. Bottom panel: relative deviation $(k_2^{\text{fluid}} - k_2^{\text{elastic}})/k_2^{\text{elastic}}$.

on the observable tidal coefficient $\Lambda_2 \propto k_2 R^5$ is the same as on k_2 since elasticity only enters through the tidal perturbations; R refers to the radius of the unperturbed (spherical) star and therefore remains unchanged. Crystallization could thus be important when analyzing the GW signals from WD binaries that will be observed by space-based GW detectors.

To conclude this section, let us now explore the situation in which the star is not entirely crystallized, i.e., a fluid layer is present on top of the solid core. In Fig. 7, we show

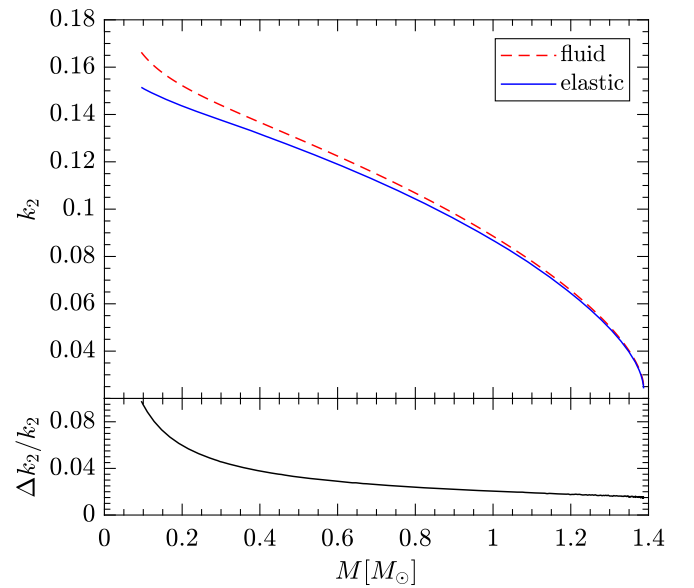
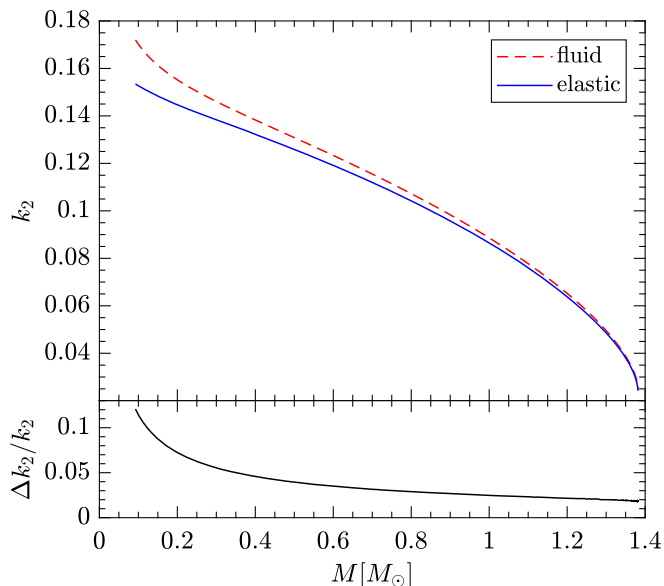
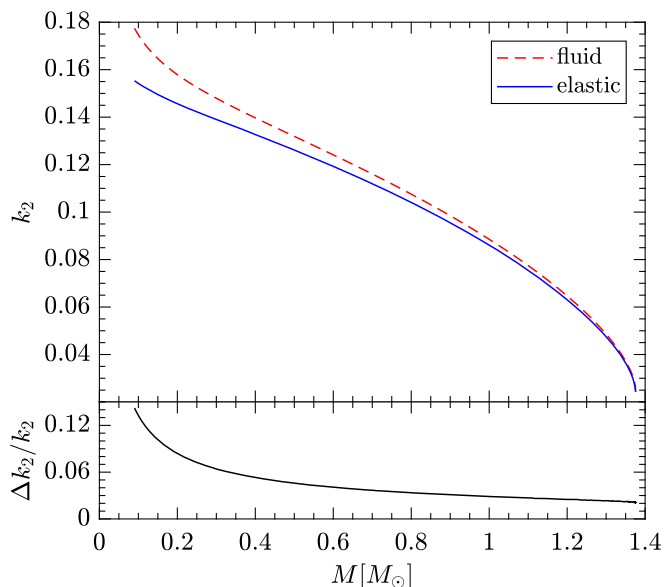
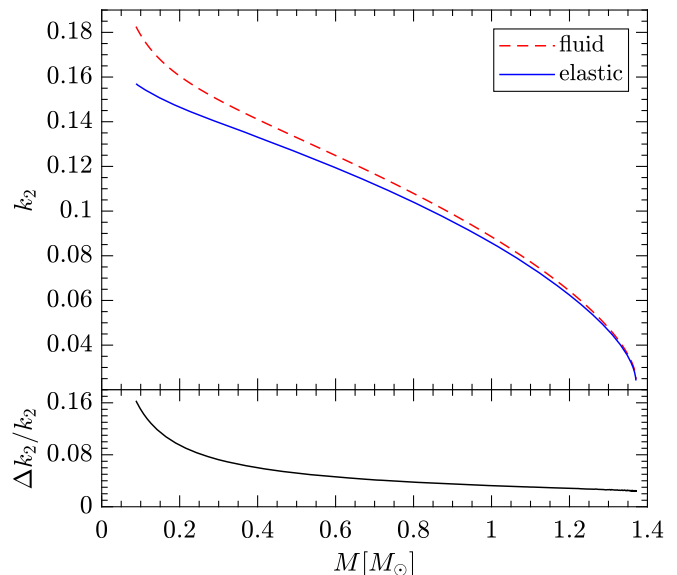


FIG. 2. Same as Fig. 1, for a WD made of ${}^{12}\text{C}$.

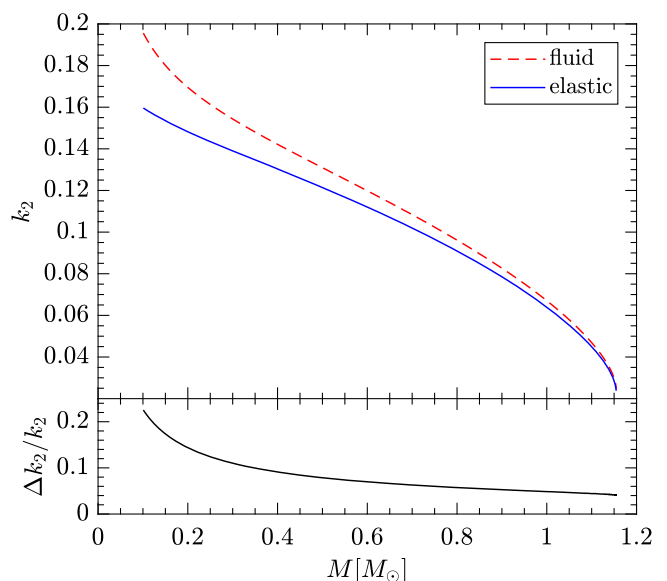
FIG. 3. Same as Fig. 1, for a WD made of ^{16}O .

the Love number k_2 for a typical $0.45 M_\odot$ oxygen WD, varying the mass-energy density $\rho_{\text{interface}}$ delimiting the interface between the two regions. In this case, k_2 (and therefore Λ_2) remains unchanged if the transition lies at densities below $\sim 10^3 \text{ g cm}^{-3}$, corresponding to a very thin fluid layer with a thickness of about 80 km, as can be seen in Fig. 8. On the other hand, k_2 is essentially given by that of a purely fluid star if only the innermost region of the core down to about 10^6 g cm^{-3} is solid. Similar conclusions hold for different compositions and masses. This shows that the actual tidal deformability of binary WDs will depend on the extent of the crystallization region.

FIG. 4. Same as Fig. 1, for a WD made of ^{20}Ne .FIG. 5. Same as Fig. 1, for a WD made of ^{24}Mg .

C. Deviations between Newtonian theory and general relativity

In this section, we compare our general-relativistic results with those obtained for purely fluid stars in Newtonian gravity. Note that GR changes not only k_2 but also R , as shown in Fig. 9 for different WDs compositions and masses. For low-mass WDs, the deviations for both k_2 and the observable combination $k_2 R^5$ are small, as one can see in Figs. 10 and 11, respectively. The relative error on $k_2 R^5$ for a typical oxygen $0.45 M_\odot$ WD is 0.48%, which is about an order of magnitude smaller than the deviation due to elasticity (4.3%). On the other hand,

FIG. 6. Same as Fig. 1, for a WD made of ^{56}Fe .

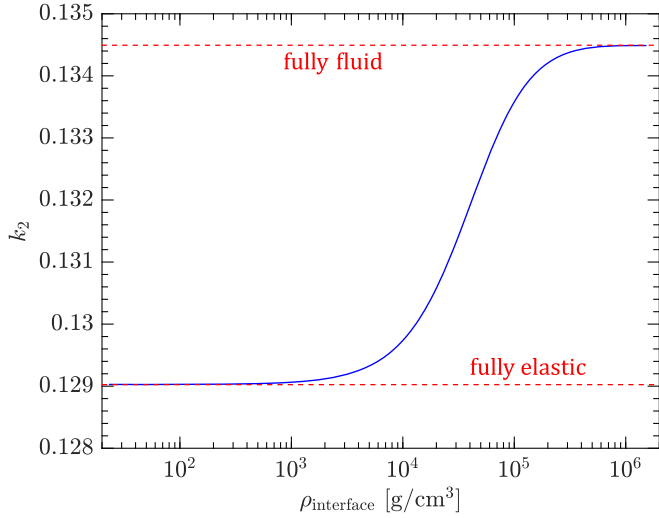


FIG. 7. Second gravitoelectric Love number k_2 as a function of the mass-energy density $\rho_{\text{interface}}$ at the interface between the elastic and fluid regions, for a $0.45 M_{\odot}$ WD made of ^{16}O . The horizontal dotted lines correspond to the two extreme cases where the star is either fully crystallized (elastic) or fully fluid.

the deviations increase with increasing mass. Although the separate corrections for k_2 and R still lie within $\sim 10\%$ for WDs with a mass $M \gtrsim 1 M_{\odot}$, that for the observable tidal deformability exceeds $\sim 10\%$ and reaches $\sim 100\%$ at the Chandrasekhar limit. Therefore, calculations in full GR become essential for the most massive WDs.

To conclude this section, we have compared our numerical results for k_2^{N} calculated with the full equation of state (7) for WDs at the Chandrasekhar limit with different compositions. Since the polytropic approximation (51) with $\Gamma = 4/3$ becomes more accurate with increasing density, we expect k_2^{N} to be independent of the mass and

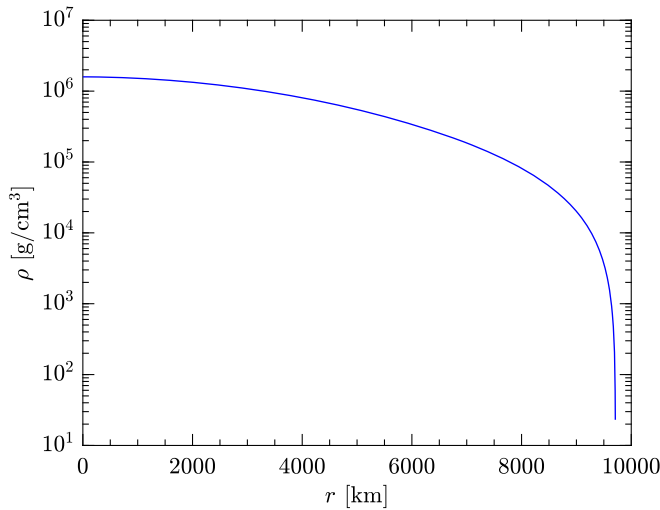


FIG. 8. Mass-energy density ρ as a function of the radial coordinate r , for a $0.45 M_{\odot}$ WD made of ^{16}O .

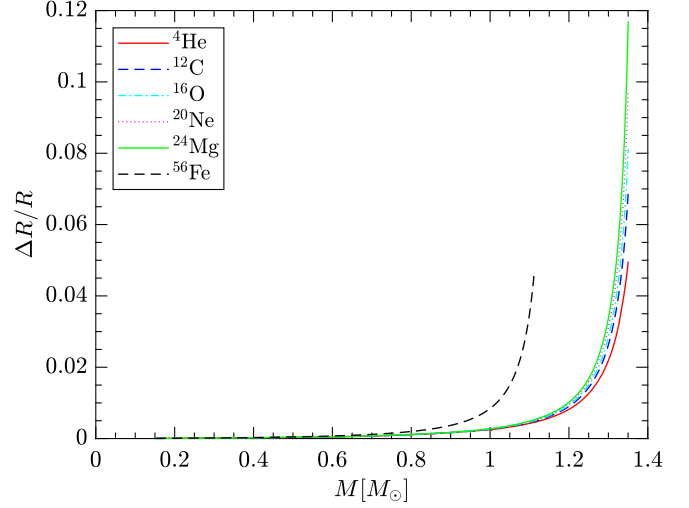


FIG. 9. Relative deviation between the star radius R calculated in full GR and in Newtonian theory $(R^{\text{N}} - R^{\text{GR}})/R^{\text{GR}}$, as a function of the WD mass M for different compositions.

internal composition of the WD, and to converge towards the universal value $k_2^{\text{N}} \simeq 0.01444298$ [66], as shown in Sec. IV A 2. We have checked that this is indeed the case with a precision of at least five significant digits.

D. Eccentric binaries

In this section, we focus on eccentric WD binary systems, which are of particular interest to extract the second gravitoelectric Love number from the GW signal. Indeed, the precession rate of the periastron could be measured through the frequency splitting of the signal, as discussed in Sec. I. The total apsidal precession rate $\dot{\gamma}$ of the binary is the sum of different contributions:

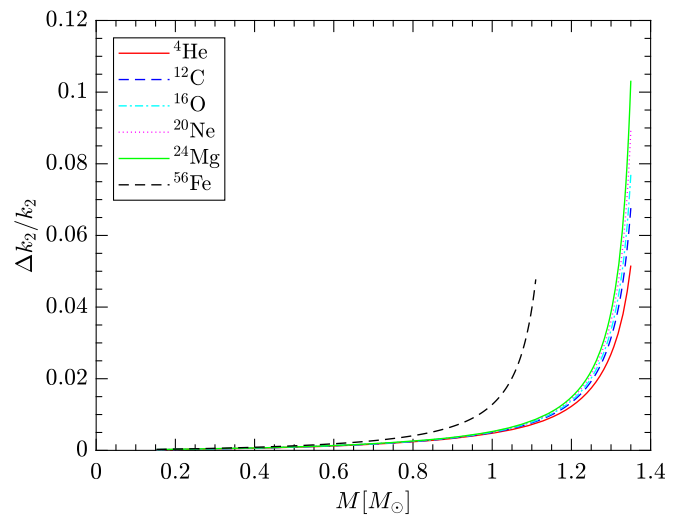


FIG. 10. Relative deviation between the Love number calculated in full GR and in Newtonian theory $(k_2^{\text{N}} - k_2^{\text{GR}})/k_2^{\text{GR}}$, as a function of the WD mass M for different compositions.

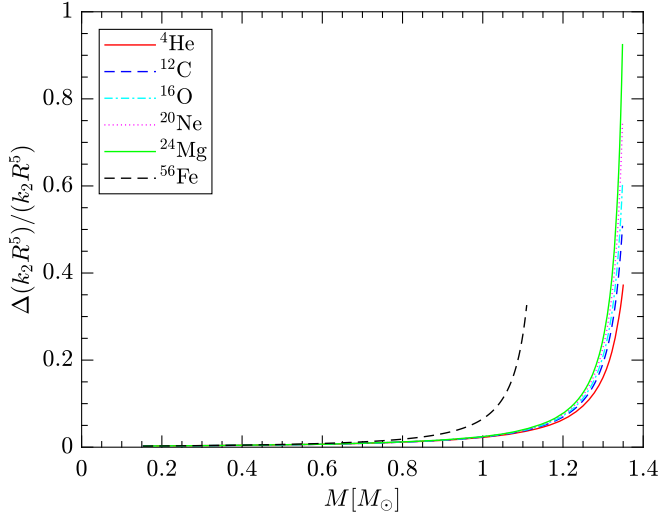


FIG. 11. Relative deviation between k_2R^5 calculated in full GR and in Newtonian theory $[(k_2R^5)^N - (k_2R^5)^{GR}]/(k_2R^5)^{GR}$, as a function of the WD mass M for different compositions.

$$\dot{\gamma} = \dot{\gamma}_{GR} + \sum_{i=1,2} \dot{\gamma}_{rot,i} + \dot{\gamma}_{tid,i}, \quad (60)$$

where $\dot{\gamma}_{GR}$ comes from GR, $\dot{\gamma}_{rot,i}$ from the rotation, and $\dot{\gamma}_{tid,i}$ from the tidal effects in each star, and the index $i = 1, 2$ is used to label the individual stars. These contributions are, respectively, given by [14]

$$\dot{\gamma}_{GR} = \left(\frac{2\pi}{T_{orb}}\right)^{5/3} \frac{3G^{2/3} M_{tot}^{2/3}}{c^2 (1-e^2)}, \quad (61)$$

$$\dot{\gamma}_{rot,i} = \frac{2\pi}{T_{orb}} \frac{1}{a^5} \frac{M_{tot}}{M_i} \frac{(\Omega_i/\Omega)^2}{(1-e^2)^2} (k_2R^5)_i, \quad (62)$$

$$\dot{\gamma}_{tid,i} = \frac{30\pi}{T_{orb}} \frac{1}{a^5} \frac{M_{3-i}}{M_i} \frac{1+3e^2/2+e^4/8}{(1-e^2)^5} (k_2R^5)_i, \quad (63)$$

where $\Omega = 2\pi/T_{orb}$ is the mean motion, Ω_i are the angular velocities of the uniformly rotating stars, M_i are the individual masses and $M_{tot} = M_1 + M_2$ is the total mass of the binary, T_{orb} is the orbital period, a is the semimajor axis of the elliptic orbit, and e is the eccentricity. For simplicity, in our calculations we assume that the rotations of the two stars are tidally locked, i.e., $\Omega_i = \Omega$ as in Ref. [14]. While the GR contribution is only a function of the orbital parameters and the total mass of the system, the rotational and tidal ones depend in addition on the individual masses as well as the internal structure of the WDs through the parameters $(k_2R^5)_i$. The sum of the tidal and rotational contributions to the precession rate must represent at least $\sim 10\%$ of the total precession rate $\dot{\gamma}$ to be observable by LISA [14], which requires the two orbiting stars to be sufficiently close to merger. The merger time of an initially eccentric binary system at formation is roughly given by [69]

$$\tau \approx 9.829 \times 10^{-3} \left(\frac{T_{orb}^0}{1 \text{ h}}\right)^{8/3} \left(\frac{M_{tot}}{M_{\odot}}\right)^{1/3} \left(\frac{M_{\odot}^2}{M_1 M_2}\right) F(e_0) \text{ Gyr}, \quad (64)$$

where T_{orb}^0 is the initial orbital period, and $F(e_0) \approx (1-e_0^2)^{7/2}$ with e_0 being the initial eccentricity. Note that for a circular orbit, $F(e_0 = 0) = 1$. The more eccentric the orbit, the shorter the merger time: for $e_0 = 0.6$, $F(e_0) \approx 0.2$ and the merger time is divided by 5 compared to a circular orbit. Depending on T_{orb}^0 and e_0 , the binaries that will be observed by LISA may have evolved for billions of years since their formation. In Fig. 12, we show the initial eccentricity e_0 as a function of the initial period of the binary T_{orb}^0 , which can be estimated from Eq. (64) for any given merger time τ :

$$e_0 \approx \sqrt{1 - \left[1.017 \times 10^2 \left(\frac{\tau}{1 \text{ Gyr}}\right) \left(\frac{T_{orb}^0}{1 \text{ h}}\right)^{-8/3} \left(\frac{M_1 M_2}{M_{\odot}^2}\right) \left(\frac{M_{tot}}{M_{\odot}}\right)^{-1/3}\right]^{2/7}}. \quad (65)$$

The shaded area between the two curves represents the binaries with a merger time between 5 and 11 Gyr, a long enough time for the interior of the WDs to have crystallized at least partially. Their initial orbital periods lie in the range predicted by population synthesis models [6]. Taking into account 2 Gyr of formation [6], these binaries are now potentially close enough to merger for tidal effects to be measurable by LISA provided the frequency of the GW signal emitted by the binary lies in the sensitivity band

10^{-4} – 10^{-1} Hz. The frequency of maximum GW power emission is approximately given by [70]

$$f_{max} \approx \frac{\sqrt{GM_{tot}}}{\pi} \frac{(1+e)^{1.1954}}{[a(1-e^2)]^{3/2}}. \quad (66)$$

To determine the current orbital properties of binary WDs that fulfill all of the above conditions, we must solve

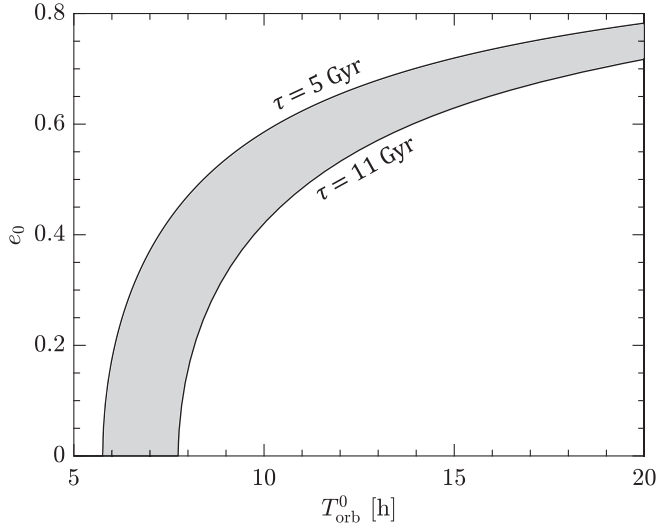


FIG. 12. Initial eccentricity e_0 as a function of the initial period T_{orb}^0 (in hours) for a binary system with two $0.45 M_{\odot}$ WDs. The shaded area represents the binaries with a merger time between 5 and 11 Gyr.

the equations governing the evolution of the semimajor axis a and the eccentricity e with time [69]:

$$\dot{a} = -\frac{64 G^3}{5 c^5} M_1 M_2 M_{\text{tot}} \frac{1}{a^3 (1-e^2)^{7/2}} \left(1 + \frac{73}{24} e^2 + \frac{37}{96} e^4 \right), \quad (67)$$

$$\dot{e} = -\frac{304 G^3}{15 c^5} M_1 M_2 M_{\text{tot}} \frac{e}{a^4 (1-e^2)^{5/2}} \left(1 + \frac{121}{304} e^2 \right), \quad (68)$$

with the semimajor axis of the elliptic orbit being linked to the orbital period through Kepler's law,

$$T_{\text{orb}} = 2\pi \sqrt{\frac{a^3}{GM_{\text{tot}}}}. \quad (69)$$

In Table I, we show some examples of equal-mass eccentric binary WDs with different compositions. Starting from an initial eccentricity of 0.60 and an initial orbital period of a few hours, we find that binaries will merge in a time between 5 and 11 Gyr. As explained before, the binary has to be close enough to merger now in order for $\dot{\gamma}_{\text{rot}} = \sum_{i=1,2} \dot{\gamma}_{\text{rot},i}$ and $\dot{\gamma}_{\text{tid}} = \sum_{i=1,2} \dot{\gamma}_{\text{tid},i}$ to represent a sizable fraction of $\dot{\gamma}$. Such a situation is encountered a few million years before the merger for very low-mass WDs. For more massive WDs, the corresponding time is shorter. This justifies our neglect of tidal effects in the evolution of the orbital parameters a and e in Eqs. (67) and (68). Even though the eccentricity has been considerably reduced at this time, it remains measurable (see Ref. [14]). Moreover, the semimajor axis length is about 1 order of magnitude larger than the radii of the stars, and therefore the perturbative approach to compute tidal effects remains

TABLE I. Parameters of potentially observable configurations of equal-mass WD binaries made of helium ($0.3\text{--}0.3 M_{\odot}$), carbon ($0.45\text{--}0.45 M_{\odot}$), or oxygen ($0.6\text{--}0.6 M_{\odot}$): initial eccentricity e_0 , and initial orbital period T_{orb}^0 at formation of the binary, merger time τ since formation of the binary, remaining time before merger $\tau - t$, current eccentricity e , current semimajor axis length a , current orbital period T_{orb} , frequency of maximum GW power emission f_{max} , and precession rates due to GR ($\dot{\gamma}_{\text{GR}}$), rotation ($\dot{\gamma}_{\text{rot}}$), and tidal effects ($\dot{\gamma}_{\text{tid}}$) using values of $k_2 R^5$ from full GR calculations with the equation of state (7) and taking crystallization into account.

Composition	${}^4\text{He}$	${}^{12}\text{C}$	${}^{16}\text{O}$
$M_{\text{tot}} [M_{\odot}]$	0.60	0.90	1.20
e_0	0.60	0.60	0.60
T_{orb}^0 [h]	10.0	13.0	16.0
τ [Gyr]	8.813	9.026	9.721
$\tau - t$ [Myr]	6.00	1.50	0.350
e	0.0393	0.0225	0.0123
a [10^5 km]	1.50	1.44	1.24
T_{orb} [h]	0.360	0.275	0.191
f_{max} [mHz]	1.62	2.07	2.96
$\dot{\gamma}_{\text{GR}}$ [yr^{-1}]	2.71	5.54	12.4
$\dot{\gamma}_{\text{rot}}$ [yr^{-1}]	0.279	0.155	0.194
$\dot{\gamma}_{\text{tid}}$ [yr^{-1}]	2.11	1.17	1.45

valid. In these examples, the frequency (66) of maximum GW power emission emitted by the system at the time of observation is of the order of a few millihertz, which lies in the LISA sensitivity band.

As previously discussed in Ref. [14], the precession rate measurement through the GW signal can be used to determine the individual masses of the WDs composing the binary system. For this purpose, it is necessary to use a relation between the observable combinations $(k_2 R^5)_i$ and the masses. In turn, this relation depends on the internal properties of the WDs. We have investigated the errors made on the inferred masses incurred by the neglect of crystallization. Since the radius is determined by the unperturbed configuration, it does not change when taking elasticity into account. Therefore, we focus on the relation between k_2 and M . We find that the numerical results can be well fitted by the following fitting formula:

$$k_2 = \sum_{j=0}^6 b_j M^j, \quad (70)$$

with the mass M in solar units. The fitting parameters b_j for fluid and elastic stars are given in Table II. The relative

TABLE II. Fitting coefficients of Eq. (70) for a WD made of ${}^{16}\text{O}$.

	b_0	b_1	b_2	b_3	b_4	b_5	b_6
Fluid	0.2005	-0.4338	1.6327	-3.8664	5.0183	-3.3791	0.9165
Elastic	0.1653	-0.1660	0.5015	-1.2012	1.5374	-1.0252	0.2748

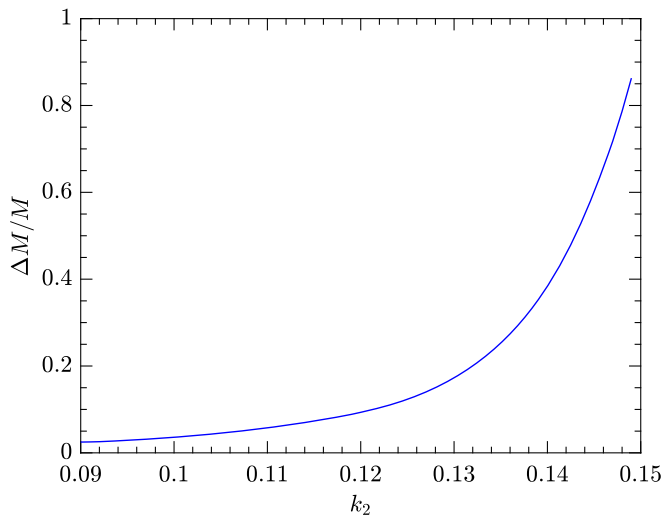


FIG. 13. Relative deviation of the mass $(M^{\text{fluid}} - M^{\text{elastic}})/M^{\text{elastic}}$ for a WD made of ^{16}O as a function of the Love number k_2 .

error on the fit is $\lesssim 0.1\%$ for WD masses between 0.1 and $1 M_{\odot}$. As shown in Fig. 13, the relative error on the mass when the elasticity of a crystallized oxygen WD is ignored becomes larger and larger when k_2 increases, i.e., for low-mass stars, and reaches about 90% for $k_2 = 0.15$. Ignoring the effects of crystallization on the tidal deformability may lead to dramatic errors when trying to deduce the individual masses from the relations (62) and (63).

V. CONCLUSIONS

Some of the WD binaries that will be observed by space-based GW detectors could have evolved for long enough for the WDs to be at least partially crystallized. We have investigated the role of crystallization in the quadrupolar tidal perturbations in binary WD systems. These perturbations, characterized by the apsidal motion constant (second gravitoelectric tidal Love number) k_2 , will be potentially measurable by LISA, which is expected to be in operation within the next decade.

We have found that the inclusion of elasticity systematically reduces the tidal deformability. This effect is more pronounced for low-mass WDs whose solid core contains heavy elements. Observations of tidal effects could thus potentially shed light on elusive iron WDs. Crystallization can lead to deviations in the tidal perturbations that are comparable or larger than the estimated observational uncertainties. This may have important implications for the analysis of the GW data from space-based detectors since most of the WDs observable with GWs are expected to have low masses.

We have also compared fully relativistic results with Newtonian ones. We have found that the general-relativistic correction to the tidal deformability remains negligible for low-mass stars compared with the correction due to elasticity. However, approaching the maximum mass, the relativistic

effects become less and less negligible. Not only is the tidal Love number k_2 affected, but also the radius R of the star.

Finally, we have focused on eccentric binary WD systems, which are of particular interest when studying tidal effects, since the precession of the periastron leads to a frequency splitting of the GW signal depending on the tidal deformabilities of the two stars. In particular, if the binary is close enough to merger, measuring this effect in the GW signal would provide the individual star masses. We have found that neglecting the elasticity of crystallized matter can lead to very large errors on the inferred masses, especially for low-mass stars.

In our work, we have considered WDs with uniform compositions. However, we do not expect that allowing for the coexistence of different elements in WDs would change our conclusions since the pressure is mainly determined by the electron gas and the shear modulus of solid compounds are not much different from those of the separate pure solids. The equation of state we have adopted here assumes fully ionized matter and complete degeneracy of the electron gas, and ignores thermal effects. Although these approximations are expected to be fairly accurate for the dense core of crystallized WDs, they become less reliable in the outermost layers. Their impact on the tidal deformability, especially for low-mass WDs, remains to be investigated using more realistic equations of state.

We have shown that the role of crystallization in tidal perturbations depends on the extent of the solid core. On the other hand, the cooling of the WDs and the crystallization may be influenced by tidal heating, especially for WDs close to merger [71]. This issue could be studied by performing cooling simulations combined with orbital evolution of the binary.

ACKNOWLEDGMENTS

The authors thank J. P. Pereira and F. Gittins for valuable discussions, and E.ourgoulhon for his kind help regarding SageMath. This work was financially supported by Fonds de la Recherche Scientifique (Belgium) and the European Cooperation in Science and Technology Action (EU) CA16214. L. P. is a FRIA grantee of the Fonds de la Recherche Scientifique (Belgium).

APPENDIX A: TAYLOR EXPANSIONS AT THE STELLAR CENTER

To start the integration of the system of equations, we need some initial conditions. Since the equations are singular at the center of the star due to terms in $\sim 1/r$, we have to expand each function in Taylor series near the center.

First, we expand the background functions:

$$P = P_c + P^{(2)}r^2 + \mathcal{O}(r^4), \quad (\text{A1a})$$

$$\rho = \rho_c + \rho^{(2)}r^2 + \mathcal{O}(r^4), \quad (\text{A1b})$$

$$m = r^3[m^{(0)} + m^{(2)}r^2 + \mathcal{O}(r^4)], \quad (\text{A1c})$$

$$\lambda = \lambda^{(0)} + \lambda^{(2)}r^2 + \mathcal{O}(r^4), \quad (\text{A1d})$$

$$\nu = \nu^{(0)} + \nu^{(2)}r^2 + \mathcal{O}(r^4). \quad (\text{A1e})$$

Inserting these expansions into Eq. (16) and the TOV equations (17) leads to the following expressions for the different coefficients:

$$P^{(2)} = -\frac{2G}{3c^4}\pi(P_c + \varepsilon_c)(3P_c + \varepsilon_c), \quad (\text{A2a})$$

$$\rho^{(2)} = \frac{P^{(2)}}{c^2\zeta_c}, \quad (\text{A2b})$$

$$m^{(0)} = \frac{4}{3}\pi\rho_c, \quad (\text{A2c})$$

$$m^{(2)} = \frac{4}{5}\pi\rho^{(2)}, \quad (\text{A2d})$$

$$\lambda^{(0)} = 0, \quad (\text{A2e})$$

$$\lambda^{(2)} = \frac{8G}{3c^2}\pi\rho_c, \quad (\text{A2f})$$

$$\nu^{(2)} = \frac{4G}{3c^4}\pi(3P_c + \varepsilon_c), \quad (\text{A2g})$$

where $\varepsilon_c = \rho_c c^2$ and $\zeta_c = \frac{1}{c^2} \frac{dP}{d\rho} |_{r=0}$ is the dimensionless speed of sound evaluated at the center of the star. The coefficient $\nu^{(0)}$ can be left arbitrary.

Next, we expand the perturbation functions:

$$H_0 = r^\ell [H_0^{(0)} + H_0^{(2)}r^2 + \mathcal{O}(r^4)], \quad (\text{A3a})$$

$$\beta = r^{\ell-1} [\ell H_0^{(0)} + (2 + \ell)H_0^{(2)}r^2 + \mathcal{O}(r^4)], \quad (\text{A3b})$$

$$K = r^\ell [K^{(0)} + K^{(2)}r^2 + \mathcal{O}(r^4)], \quad (\text{A3c})$$

$$V = r^\ell [V^{(0)} + V^{(2)}r^2 + \mathcal{O}(r^4)], \quad (\text{A3d})$$

$$W = r^\ell [W^{(0)} + W^{(2)}r^2 + \mathcal{O}(r^4)], \quad (\text{A3e})$$

$$T_\theta = r^\ell [T_\theta^{(0)} + T_\theta^{(2)}r^2 + \mathcal{O}(r^4)]. \quad (\text{A3f})$$

We can also expand the shear modulus in the same way:

$$\tilde{\mu} = \tilde{\mu}_c + \tilde{\mu}^{(2)}r^2 + \mathcal{O}(r^4), \quad (\text{A4})$$

where $\tilde{\mu}^{(2)} = P^{(2)}\chi_c$ with $\chi_c = \frac{d\tilde{\mu}}{dP} |_{r=0}$. Inserting these expansions into the elastic equations (40) and using Eqs. (A1) with Eqs. (A2) for the background functions, we get for the zeroth-order coefficients

$$K^{(0)} = H_0^{(0)} + 32\pi \frac{G}{c^4} \tilde{\mu}_c V^{(0)}, \quad (\text{A5a})$$

$$W^{(0)} = \ell V^{(0)}, \quad (\text{A5b})$$

$$T_\theta^{(0)} = -2 \frac{G}{c^4} (\ell - 1) \tilde{\mu}_c V^{(0)}, \quad (\text{A5c})$$

and for the second-order ones,

$$\begin{aligned} H_0^{(2)} = 2\pi \frac{G}{c^4} \left\{ 32\pi \frac{G}{c^4} \zeta_c (9 + \ell) \tilde{\mu}_c^2 [3(-3 + \ell + 9\zeta_c)P_c + (3 + \ell + 27\zeta_c)\varepsilon_c] V^{(0)} \right. \\ - 9\zeta_c(3 + \ell)(P_c + \varepsilon_c) \left[(1 + 9\zeta_c + \ell\zeta_c)H_0^{(0)} - 16\pi \frac{G}{c^4} (1 + 3\zeta_c)\chi_c(-1 + \ell)P_c V^{(0)} \right] P_c \\ - 3\zeta_c(3 + \ell)(P_c + \varepsilon_c) \left[(3 + 15\zeta_c - 3\ell\zeta_c - 2\ell^2\zeta_c)H_0^{(0)} - 64\pi \frac{G}{c^4} (1 + 3\zeta_c)\chi_c(-1 + \ell)P_c V^{(0)} \right] \varepsilon_c \\ + 48\pi \frac{G}{c^4} \zeta_c(3 + \ell)(P_c + \varepsilon_c)(1 + 3\zeta_c)\chi_c(-1 + \ell)\varepsilon_c^2 V^{(0)} - 24\pi \frac{G}{c^4} \tilde{\mu}_c [\ell(9 + \ell) + 6\zeta_c^2(3 + \ell)(9 + \ell) \\ + 3\zeta_c(-6 + 13\ell + 3\ell^2)] P_c^2 V^{(0)} + 3\zeta_c \tilde{\mu}_c (-3 + 9\zeta_c - \ell)(9 + \ell) P_c H_0^{(0)} - 36\zeta_c \tilde{\mu}_c (1 + 3\zeta_c)(1 + \ell)(3 + 2\ell) P_c V^{(2)} \\ + 16\pi \frac{G}{c^4} \tilde{\mu}_c [3\zeta_c \ell(-7 + \ell)(4 + \ell) - 2\ell(9 + \ell) + 3\zeta_c^2(-144 - 54\ell + 5\ell^2 + 3\ell^3)] P_c \varepsilon_c V^{(0)} \\ + \tilde{\mu}_c \zeta_c (9 + \ell)(3 + 3\ell + 2\ell^2 + 27\zeta_c)\varepsilon_c H_0^{(0)} - 36\zeta_c \tilde{\mu}_c (1 + 3\zeta_c)(1 + \ell)(3 + 2\ell)\varepsilon_c V^{(2)} \\ + 8\pi \frac{G}{c^4} \tilde{\mu}_c [-\ell(9 + \ell) + 3\zeta_c(1 + \ell)(-18 + \ell + 2\ell^2) + 6\zeta_c^2(-63 - 18\ell + 8\ell^2 + 3\ell^3)] \varepsilon_c^2 V^{(0)} \left. \right\} \\ \times \{ 3\zeta_c(3 + 2\ell)[(9 + \ell)\tilde{\mu}_c + 3\zeta_c(3 + \ell)(P_c + \varepsilon_c)] \}^{-1}, \quad (\text{A6a}) \end{aligned}$$

$$\begin{aligned}
K^{(2)} = & 2\pi \frac{G}{c^4} \left\{ -9\zeta_c(3 + \ell)(P_c + \varepsilon_c)[2 + \ell + \zeta_c(6 + 3\ell + \ell^2)]P_c H_0^{(0)} - 144\pi \frac{G}{c^4} \zeta_c \chi_c(3 + \ell)(P_c + \varepsilon_c) \right. \\
& \times [(1 - \ell)(2 + \ell) + \zeta_c(6 + 3\ell + \ell^2)]P_c^2 V^{(0)} - 3\zeta_c(3 + \ell)(P_c + \varepsilon_c) \\
& \times [3(2 + \ell) + \zeta_c(18 + \ell - 7\ell^2 - 2\ell^3)]\varepsilon_c H_0^{(0)} - 192\pi \frac{G}{c^4} \zeta_c \chi_c(3 + \ell)(P_c + \varepsilon_c) \\
& \times [(1 - \ell)(2 + \ell) + \zeta_c(6 + 3\ell + \ell^2)]P_c \varepsilon_c V^{(0)} - 48\pi \frac{G}{c^4} \zeta_c \chi_c(3 + \ell)(P_c + \varepsilon_c) \\
& \times [(1 - \ell)(2 + \ell) + \zeta_c(6 + 3\ell + \ell^2)]\varepsilon_c^2 V^{(0)} + 16\zeta_c \tilde{\mu}_c^2 [3(3 + 2\ell)(6 + 3\ell + \ell^2)]V^{(2)} \\
& + 32\pi \frac{G}{c^4} \zeta_c \tilde{\mu}_c^2 [3(18 + 21\ell + \ell^3)P_c + 27\zeta_c(6 + 3\ell + \ell^2)P_c + (54 + 87\ell + 62\ell^2 + 17\ell^3)\varepsilon_c \\
& + 27\zeta_c(6 + 3\ell + \ell^2)\varepsilon_c]V^{(0)} - 24\pi \frac{G}{c^4} \tilde{\mu}_c [\ell(2 + \ell)(9 + \ell) + 6\zeta_c^2(3 + \ell)(6 + 3\ell + \ell^2) \\
& + 3\zeta_c(-12 + 8\ell + 11\ell^2 + 3\ell^3) + 4\zeta_c(3 + 2\ell)(6 + 3\ell + \ell^2)\chi_c]P_c^2 V^{(0)} \\
& + 3\zeta_c \tilde{\mu}_c [18 - \ell(-9 + 6\ell + \ell^2) + 9\zeta_c(6 + 3\ell + \ell^2)]P_c H_0^{(0)} \\
& + 36\zeta_c \tilde{\mu}_c(3 + 2\ell)[(-1 - \ell)(2 + \ell) + \zeta_c(6 + 3\ell + \ell^2)]P_c V^{(2)} \\
& + 16\pi \frac{G}{c^4} \tilde{\mu}_c [-2\ell(2 + \ell)(9 + \ell) + 3\zeta_c \ell(-32 - 18\ell - \ell^2 + \ell^3) \\
& + 3\zeta_c^2(4 + \ell)(-36 - 12\ell + 7\ell^2 + 3\ell^3) - 8\zeta_c(3 + 2\ell)(6 + 3\ell + \ell^2)\chi_c]P_c \varepsilon_c V^{(0)} \\
& + \zeta_c \tilde{\mu}_c [54 + \ell(99 + 80\ell + 25\ell^2 + 2\ell^3) + 27\zeta_c(6 + 3\ell + \ell^2)]\varepsilon_c H_0^{(0)} \\
& + 36\zeta_c \tilde{\mu}_c(3 + 2\ell)[(-1 - \ell)(2 + \ell) + \zeta_c(6 + 3\ell + \ell^2)]\varepsilon_c V^{(2)} \\
& + 8\pi \frac{G}{c^4} \tilde{\mu}_c [-\ell(2 + \ell)(9 + \ell) + 3\zeta_c(-36 - 40\ell - 3\ell^2 + 7\ell^3 + 2\ell^4) \\
& + 6\zeta_c^2(-90 - 39\ell + 34\ell^2 + 22\ell^3 + 3\ell^4) - 4\zeta_c(3 + 2\ell)(6 + 3\ell + \ell^2)\chi_c]\varepsilon_c^2 V^{(0)} \left. \right\} \\
& \times \{3\zeta_c(2 + \ell)(3 + 2\ell)[(9 + \ell)\tilde{\mu}_c + 3\zeta_c(3 + \ell)(P_c + \varepsilon_c)]\}^{-1}, \tag{A6b}
\end{aligned}$$

$$\begin{aligned}
W^{(2)} = & \left\{ 6\tilde{\mu}_c(-6 + \ell)(1 + \ell)V^{(2)} + 16\pi \frac{G}{c^4} \tilde{\mu}_c [-9(-1 + \ell + 6\zeta_c)P_c - (9 + 4\ell - 3\ell^2 + 54\zeta_c)\varepsilon_c]V^{(0)} \right. \\
& - 9(1 + 3\zeta_c)(P_c + \varepsilon_c)H_0^{(0)} + 18\zeta_c \ell(1 + \ell)(P_c + \varepsilon_c)V^{(2)} + 24\pi \frac{G}{c^4} (P_c + \varepsilon_c) \\
& \times [3(\ell - 2\chi_c + 2\ell\chi_c)P_c + (\ell - 2\zeta_c \ell - 2\chi_c + 2\ell\chi_c)\varepsilon_c]V^{(0)} \left. \right\} \\
& \times \{6[(9 + \ell)\tilde{\mu}_c + 3\zeta_c(3 + \ell)(P_c + \varepsilon_c)]\}^{-1}, \tag{A6c}
\end{aligned}$$

$$\begin{aligned}
T_\theta^{(2)} = & \frac{G}{c^4} \left\{ 24\pi \frac{G}{c^4} \zeta_c(-1 + \ell)(3 + \ell)\chi_c(P_c + \varepsilon_c)^2(3P_c + \varepsilon_c)V^{(0)} - 12\tilde{\mu}_c^2(-1 + \ell)(3 + \ell)V^{(2)} \right. \\
& + 16\pi \frac{G}{c^4} \tilde{\mu}_c^2 [9(-1 + \ell + 6\zeta_c)P_c + (9 - 5\ell - 4\ell^2 + 54\zeta_c)\varepsilon_c]V^{(0)} \\
& + 9\tilde{\mu}_c(P_c + \varepsilon_c)[(1 + 3\zeta_c)H_0^{(0)} - 4\zeta_c \ell(2 + \ell)V^{(2)}] + 8\pi \frac{G}{c^4} \tilde{\mu}_c(P_c + \varepsilon_c) \\
& \times [-9\ell P_c - 3\ell(1 + 4\zeta_c + 2\zeta_c \ell)\varepsilon_c + (-1 + \ell)(3 + \ell)\chi_c(3P_c + \varepsilon_c)]V^{(0)} \left. \right\} \\
& \times \{6[(9 + \ell)\tilde{\mu}_c + 3\zeta_c(3 + \ell)(P_c + \varepsilon_c)]\}^{-1}. \tag{A6d}
\end{aligned}$$

We note that we only have seven constraints for ten unknown coefficients. The remaining coefficients can be determined as discussed in Sec. IV A 1.

APPENDIX B: EQUIVALENCE BETWEEN LOVE NUMBER AND APSIDAL-MOTION CONSTANT

In this appendix, we show that the apsidal-motion constants [72] considered in previous (Newtonian) studies of binary WDs [12–14] are equivalent to Love numbers [73]. Introducing the function $y(r) = r\beta(r)/H_0(r)$, we can rewrite the perfect-fluid perturbation equation (41) together with (40c) as a single first-order differential equation:

$$\begin{aligned} ry' + y^2 + e^\lambda \left[1 + 4\pi \frac{G}{c^4} r^2 (P - \rho c^2) \right] y \\ + 4\pi \frac{G}{c^4} r^2 e^\lambda \left(9P + 5\rho c^2 + \frac{P + \rho c^2}{c_s^2} c^2 \right) \\ - \ell(\ell + 1) e^\lambda - r^2 \nu^2 = 0. \end{aligned} \quad (\text{B1})$$

If the density ρ does not vanish at the surface of the star [defined by $P(R) = 0$], one has to add a correction to $y(R)$ calculated from Eq. (B1). It can be obtained from the boundary conditions (49) and (50), and using the fact that $\delta P = \frac{\rho c^2 + P}{2} H_0$ [from Eq. (29e) in Ref. [32]] in a fluid region,

$$y^+(R) = y^-(R) - 3 \frac{\rho^-(R)}{\bar{\rho}(R)}, \quad (\text{B2})$$

where $\bar{\rho}(r) = \frac{3}{4\pi r^3} m(r)$ is the average mass-energy density inside a sphere of radius r .

In the Newtonian limit, Eq. (B1) reduces to

$$ry' + y(y + 1) - \ell(\ell + 1) + \frac{4\pi G r^2 \rho_N}{c_s^2} = 0. \quad (\text{B3})$$

Making the change of variable

$$y(r) = \eta(r) + 3 \frac{\rho_N(r)}{\bar{\rho}_N(r)} - 1, \quad (\text{B4})$$

and using the hydrostatic equilibrium equations (18a)–(18b), we recover the so-called Clairaut-Radau differential equation for the variable η [see Eq. (5) of Ref. [72]]:

$$\eta' + \eta(\eta - 1) - \ell(\ell + 1) + 6 \frac{\rho_N}{\bar{\rho}_N} (\eta + 1) = 0. \quad (\text{B5})$$

The surface boundary condition (B2) remains the same except that the mass-energy density ρ should be replaced by the mass density ρ_N :

$$y^+(R) = y^-(R) - 3 \frac{\rho_N^-(R)}{\bar{\rho}_N(R)}. \quad (\text{B6})$$

With this and Eq. (B4) evaluated at $r = R$, and inserting $y^+(R)$ into Eq. (46), we recover the explicit expression for the Newtonian apsidal-motion constant for $\ell = 2$ [see Eq. (1) in Ref. [66]]:

$$k_2^N = \frac{3 - \eta(R)}{4 + 2\eta(R)}. \quad (\text{B7})$$

-
- [1] M. Bailes *et al.*, *Nat. Rev. Phys.* **3**, 344 (2021).
[2] P. Amaro-Seoane *et al.*, arXiv:2203.06016.
[3] S. Kawamura *et al.*, *Prog. Theor. Exp. Phys.* **2021**, 05A105 (2021).
[4] Y. Gong, J. Luo, and B. Wang, *Nat. Astron.* **5**, 881 (2021).
[5] V. Korol, E. M. Rossi, P. J. Groot, G. Nelemans, S. Toonen, and A. G. A. Brown, *Mon. Not. R. Astron. Soc.* **470**, 1894 (2017).
[6] A. Lamberts, S. Blunt, T. B. Littenberg, S. Garrison-Kimmel, T. Kupfer, and R. E. Sanderson, *Mon. Not. R. Astron. Soc.* **490**, 5888 (2019).
[7] Z. Li, X. Chen, H.-L. Chen, J. Li, S. Yu, and Z. Han, *Astrophys. J.* **893**, 2 (2020).
[8] K. Breivik, S. Coughlin, M. Zevin, C. L. Rodriguez, K. Kremer, C. S. Ye, J. J. Andrews, M. Kurkowski, M. C. Digman, S. L. Larson, and F. A. Rasio, *Astrophys. J.* **898**, 71 (2020).
[9] V. Korol, N. Hallakoun, S. Toonen, and N. Karnesis, *Mon. Not. R. Astron. Soc.* **511**, 5936 (2022).
[10] B. Willems, V. Kalogera, A. Vecchio, N. Ivanova, F. A. Rasio, J. M. Fregeau, and K. Belczynski, *Astrophys. J. Lett.* **665**, L59 (2007).
[11] T. A. Thompson, *Astrophys. J.* **741**, 82 (2011).
[12] B. Willems, A. Vecchio, and V. Kalogera, *Phys. Rev. Lett.* **100**, 041102 (2008).
[13] B. Willems, A. Vecchio, and V. Kalogera, *Phys. Rev. Lett.* **101**, 219903 (2008).
[14] F. Valsecchi, W. M. Farr, B. Willems, C. J. Deloye, and V. Kalogera, *Astrophys. J.* **745**, 137 (2012).
[15] K. Maguire, M. Eracleous, P. G. Jonker, M. MacLeod, and S. Rosswog, *Space Sci. Rev.* **216**, 39 (2020).
[16] M. J. Benacquista, *Astrophys. J. Lett.* **740**, L54 (2011).
[17] S. Shah and G. Nelemans, *Astrophys. J.* **791**, 76 (2014).
[18] A. L. Piro, *Astrophys. J. Lett.* **885**, L2 (2019).

- [19] A. Wolz, K. Yagi, N. Anderson, and A. J. Taylor, *Mon. Not. R. Astron. Soc.* **500**, L52 (2021).
- [20] D. A. Kirzhnits, *Sov. Phys. JETP* **11**, 365 (1960), http://jetp.ras.ru/cgi-bin/dn/e_011_02_0365.pdf.
- [21] A. A. Abrikosov, *Sov. Phys. JETP* **12**, 1254 (1961).
- [22] E. E. Salpeter, *Astrophys. J.* **134**, 669 (1961).
- [23] D. E. Winget, S. O. Kepler, A. Kanaan, M. H. Montgomery, and O. Giovannini, *Astrophys. J. Lett.* **487**, L191 (1997).
- [24] A. H. Córscico, F. C. De Gerónimo, M. E. Camisassa, and L. G. Althaus, *Astron. Astrophys.* **632**, A119 (2019).
- [25] L. Mestel and M. A. Ruderman, *Mon. Not. R. Astron. Soc.* **136**, 27 (1967).
- [26] H. M. van Horn, *Astrophys. J.* **151**, 227 (1968).
- [27] P.-E. Tremblay, G. Fontaine, N. P. Gentile Fusillo, B. H. Dunlap, B. T. Gänsicke, M. A. Hollands, J. J. Hermes, T. R. Marsh, E. Cukanovaite, and T. Cunningham, *Nature (London)* **565**, 202 (2019).
- [28] K. Boshkayev and H. Quevedo, *Mon. Not. R. Astron. Soc.* **478**, 1893 (2018).
- [29] A. J. Taylor, K. Yagi, and P. L. Arras, *Mon. Not. R. Astron. Soc.* **492**, 978 (2020).
- [30] A. J. Penner, N. Andersson, L. Samuelsson, I. Hawke, and D. I. Jones, *Phys. Rev. D* **84**, 103006 (2011).
- [31] B. Biswas, R. Nandi, P. Char, and S. Bose, *Phys. Rev. D* **100**, 044056 (2019).
- [32] F. Gittins, N. Andersson, and J. P. Pereira, *Phys. Rev. D* **101**, 103025 (2020).
- [33] J. P. Pereira, M. Bejger, N. Andersson, and F. Gittins, *Astrophys. J.* **895**, 28 (2020).
- [34] G. Nelemans and T. M. Tauris, *Astron. Astrophys.* **335**, L85 (1998), <https://ui.adsabs.harvard.edu/abs/1998A%26A...335L..85N/abstract>.
- [35] J. Liebert, P. Bergeron, D. Eisenstein, H. C. Harris, S. J. Kleinman, A. Nitta, and J. Krzesinski, *Astrophys. J. Lett.* **606**, L147 (2004).
- [36] O. G. Benvenuto and M. A. De Vito, *Mon. Not. R. Astron. Soc.* **362**, 891 (2005).
- [37] K. Nomoto, *Astrophys. J.* **277**, 791 (1984).
- [38] J. Isern, R. Canal, and J. Labay, *Astrophys. J. Lett.* **372**, L83 (1991).
- [39] G. C. Jordan, H. B. Perets, R. T. Fisher, and D. R. van Rossum, *Astrophys. J. Lett.* **761**, L23 (2012).
- [40] J. L. Provencal, H. L. Shipman, F. Wesemael, P. Bergeron, H. E. Bond, J. Liebert, and E. M. Sion, *Astrophys. J.* **480**, 777 (1997).
- [41] J. A. Panei, L. G. Althaus, and O. G. Benvenuto, *Astron. Astrophys.* **353**, 970 (2000), <https://ui.adsabs.harvard.edu/abs/2000A%26A...353..970P/abstract>.
- [42] J. L. Provencal, H. L. Shipman, D. Koester, F. Wesemael, and P. Bergeron, *Astrophys. J.* **568**, 324 (2002).
- [43] S. Catalán, I. Ribas, J. Isern, and E. García-Berro, *Astron. Astrophys.* **477**, 901 (2008).
- [44] H. E. Bond, R. L. Gilliland, G. H. Schaefer, P. Demarque, T. M. Girard, J. B. Holberg, D. Gudehus, B. D. Mason, V. Kozhurina-Platais, M. R. Burleigh, M. A. Barstow, and E. P. Nelan, *Astrophys. J.* **813**, 106 (2015).
- [45] A. Bédard, P. Bergeron, and G. Fontaine, *Astrophys. J.* **848**, 11 (2017).
- [46] H. E. Bond, R. L. Gilliland, G. H. Schaefer, M. A. Barstow, P. Demarque, J. B. Holberg, and V. Kozhurina-Platais, *Res. Notes AAS* **2**, 147 (2018).
- [47] P. Bergeron, P. Dufour, G. Fontaine, S. Coutu, S. Blouin, C. Genest-Beaulieu, A. Bédard, and B. Rolland, *Astrophys. J.* **876**, 67 (2019).
- [48] P. Haensel, A. Y. Potekhin, and D. G. Yakovlev, *Neutron Stars. I. Equation of State and Structure* (Springer, New York, 2007).
- [49] D. A. Baiko and A. I. Chugunov, *Mon. Not. R. Astron. Soc.* **510**, 2628 (2022).
- [50] G. Gabadadze and R. A. Rosen, *J. Cosmol. Astropart. Phys.* **10** (2008) 030.
- [51] P. F. Bedaque, E. Berkowitz, and S. Sen, *Phys. Rev. D* **89**, 045010 (2014).
- [52] D. Lunney, J. M. Pearson, and C. Thibault, *Rev. Mod. Phys.* **75**, 1021 (2003).
- [53] N. Chamel and A. F. Fantina, *Phys. Rev. D* **93**, 063001 (2016).
- [54] M. Martínez-Canales, C. J. Pickard, and R. J. Needs, *Phys. Rev. Lett.* **108**, 045704 (2012).
- [55] D. A. Baiko, A. Y. Potekhin, and D. G. Yakovlev, *Phys. Rev. E* **64**, 057402 (2001).
- [56] D. A. Baiko, *Mon. Not. R. Astron. Soc.* **416**, 22 (2011).
- [57] A. I. Chugunov, *Mon. Not. R. Astron. Soc.* **500**, L17 (2021).
- [58] D. Kobyakov and C. J. Pethick, *Mon. Not. R. Astron. Soc.* **449**, L110 (2015).
- [59] T. Hinderer, *Astrophys. J.* **677**, 1216 (2008).
- [60] T. Hinderer, L. Rezzolla, and L. Baiotti, in *The Physics and Astrophysics of Neutron Stars*, Astrophysics and Space Science Library Vol. 457, edited by L. Rezzolla, P. Pizzochero, D. I. Jones, N. Rea, and I. Vidaña (Springer, Cham, 2018), pp. 575–635.
- [61] R. C. Tolman, *Phys. Rev.* **55**, 364 (1939).
- [62] J. R. Oppenheimer and G. M. Volkoff, *Phys. Rev.* **55**, 374 (1939).
- [63] T. Regge and J. A. Wheeler, *Phys. Rev.* **108**, 1063 (1957).
- [64] N. Andersson and G. L. Comer, *Living Rev. Relativity* **10**, 1 (2007).
- [65] N. Andersson, B. Haskell, G. L. Comer, and L. Samuelsson, *Classical Quantum Gravity* **36**, 105004 (2019).
- [66] R. A. Brooker and T. W. Olle, *Mon. Not. R. Astron. Soc.* **115**, 101 (1955).
- [67] S. Chandrasekhar, *An Introduction to the Study of Stellar Structure* (Dover, New York, 1957).
- [68] S. Chandrasekhar, *Astrophys. J.* **74**, 81 (1931).
- [69] M. Maggiore, *Gravitational Waves. Vol. 1: Theory and Experiments*, Oxford Master Series in Physics (Oxford University Press, New York, 2007).
- [70] L. Wen, *Astrophys. J.* **598**, 419 (2003).
- [71] A. L. Piro, *Astrophys. J. Lett.* **740**, L53 (2011).
- [72] T. E. Sterne, *Mon. Not. R. Astron. Soc.* **99**, 451 (1939).
- [73] A. E. H. Love, *Proc. R. Soc. A* **82**, 73 (1909).